remote sensing

Supplementary material for the article:

Heterogeneous Behavior of the Campotosto Normal Fault (Central Italy) Imaged by InSAR GPS and Strong-Motion Data: Insights from the 18 January 2017 Events

Daniele Cheloni[1,*], Nicola D'Agostino[1], Laura Scognamiglio[1], Elisa Tinti[1], Christian Bignami[1], Antonio Avallone [1], Roberta Giuliani[2], Stefano Calcaterra[3], Piera Gambino[3] and Maurizio Mattone[2]

[1] Istituto Nazionale di Geofisica e Vulcanologia, Via di Vigna Murata 605, 00143, Rome, Italy; nicola.dagostino@ingv.it (N.D.); laura.scognamiglio@ingv.it (L.S.); elisa.tinti@ingv.it (E.T.); christian.bignami@ingv.it (C.B.); antonio.avallone@ingv.it (A.A.);

[2] Dipartimento della Protezione Civile, Via Vitorchiano 4, 00189, Rome, Italy; roberta.giuliani@protezionecivile.it (R.G.); maurizio.mattone@protezionecivile.it (M.M.)

[3] Istituto Superiore per la Protezione e la Ricerca Ambientale, Via Vitaliano Brancati 48, 00144, Rome, Italy; stefano.calcaterra@isprambiente.it (S.C.); piera.gambino@isprambiente.it (P.G.)

* Correspondence: daniele.cheloni@ingv.it

This supplementary material consists of 7 figures and contains information about:

- confidence intervals of the best-fit uniform-slip estimated model parameters;
- observed and modelled horizontal and vertical GPS displacements with the best-fit uniform-slip model;
- the solution smoothing;
- the relative weights;
- tests on the vertical continuity of the Campotosto fault.

Supplementary figures

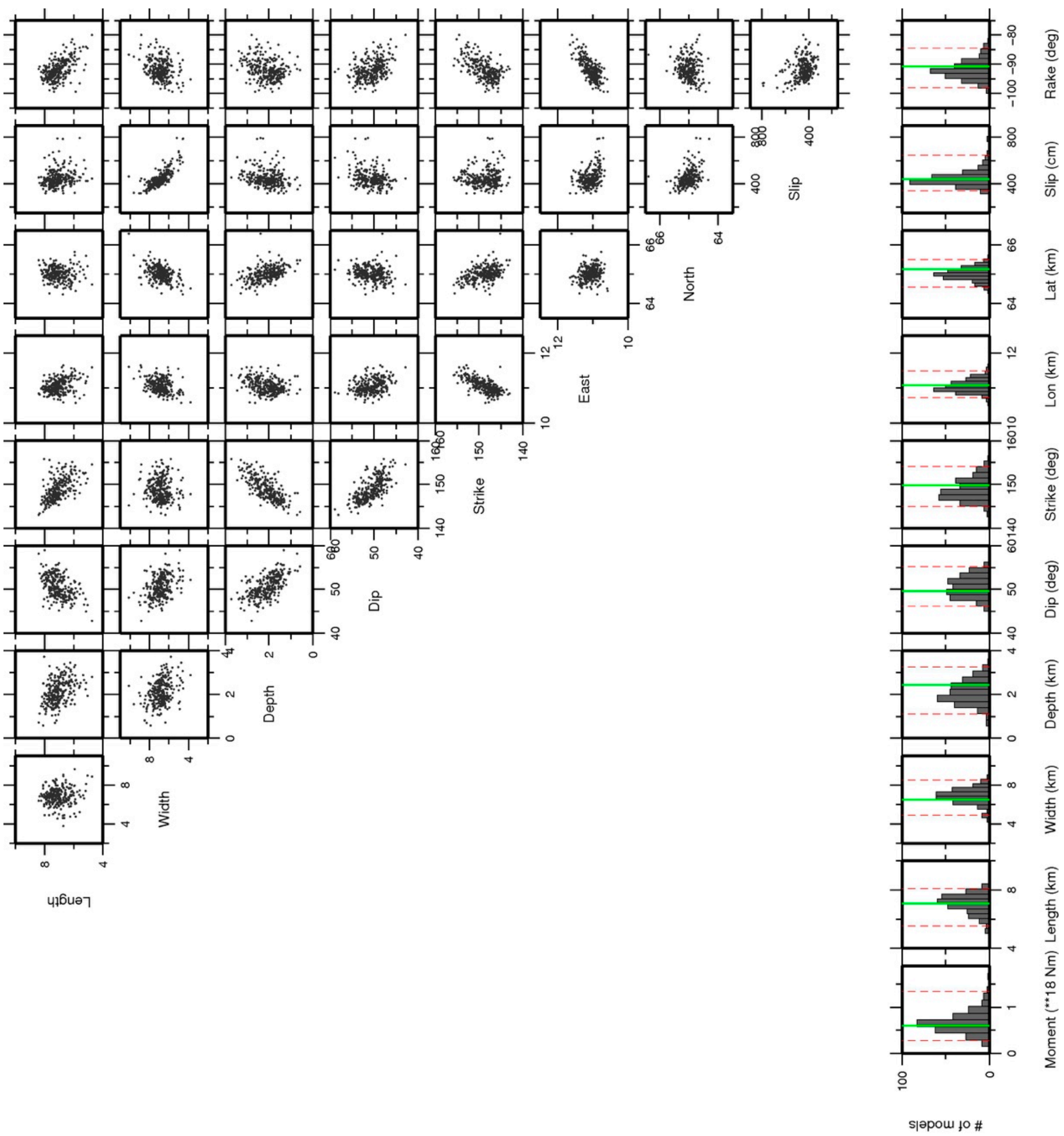

Figure S1. Trade-offs between the model parameters of the uniform-slip solution obtained by applying the best-fit technique to a large number (500) of synthetic data sets, each one derived from adding synthetic realizations of data noise to the actual data. The histograms on the bottom row show the *a-posteriori* distribution of the model parameters (the red dashed lines bracket the 95% individual confidence intervals, while the green ones show the best-fit parameter values). The other rows represent the scatter plots of the correlation between parameter pairs.

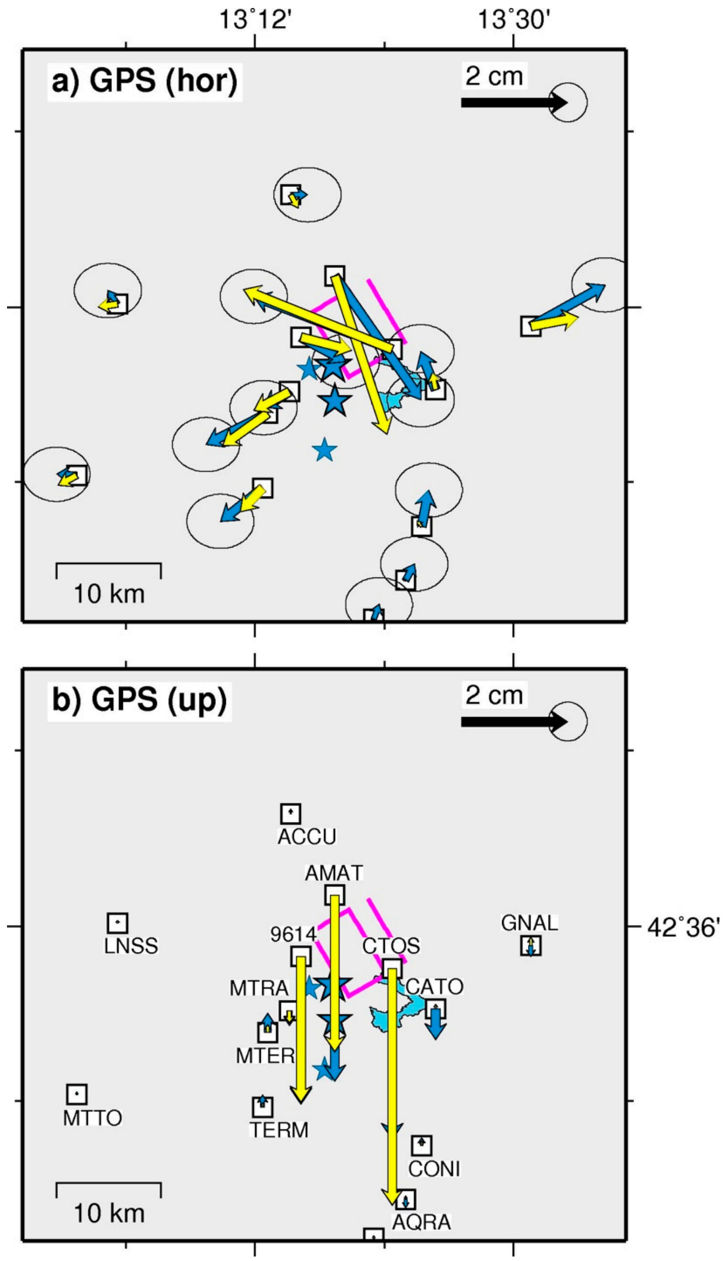

Figure 2. Observed (blue) and modelled (yellow) cumulative GPS displacements: (**a**) horizontal, and (**b**) vertical displacements, respectively. The blue stars are the four largest events of the 2017 seismic sequence. The violet box represents our best-fit uniform-slip solution.

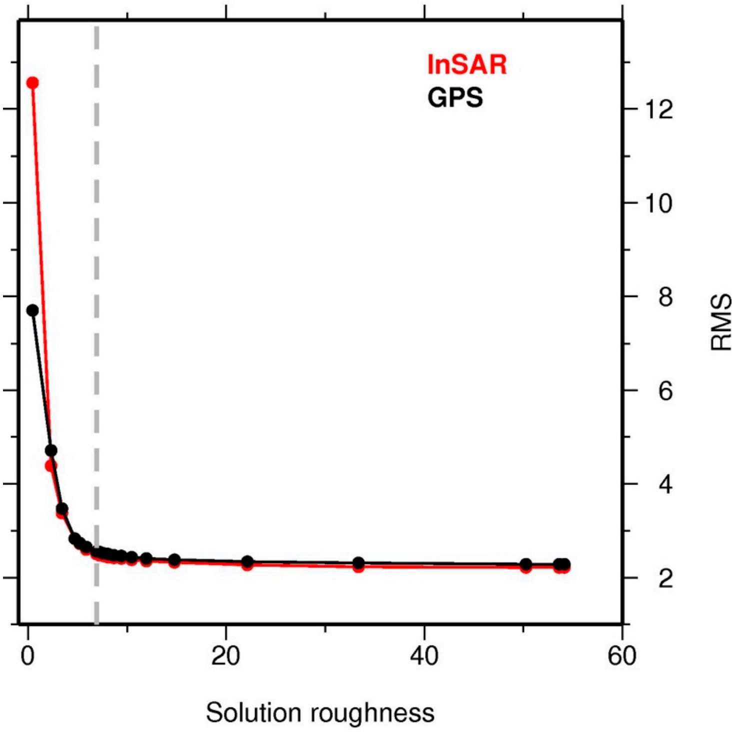

Figure 3. Trade-off curves between RMS (in mm) data and model roughness. The black circles represent the RMS of the GPS datasets, while the red ones are relevant to the InSAR measurements. The gray dashed line represents our choice of smoothing factor.

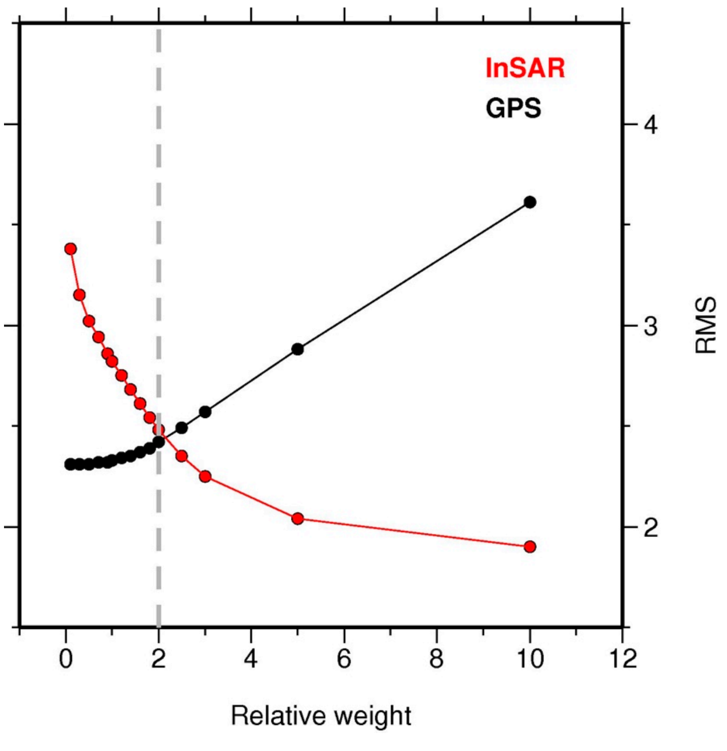

Figure 4. Relationship between RMS (in mm) data reduction and relative weighting factors. The black circles represent the RMS of the GPS datasets, while the red ones are relevant to the InSAR measurements. The gray dashed line represents our choice of weighting factor.

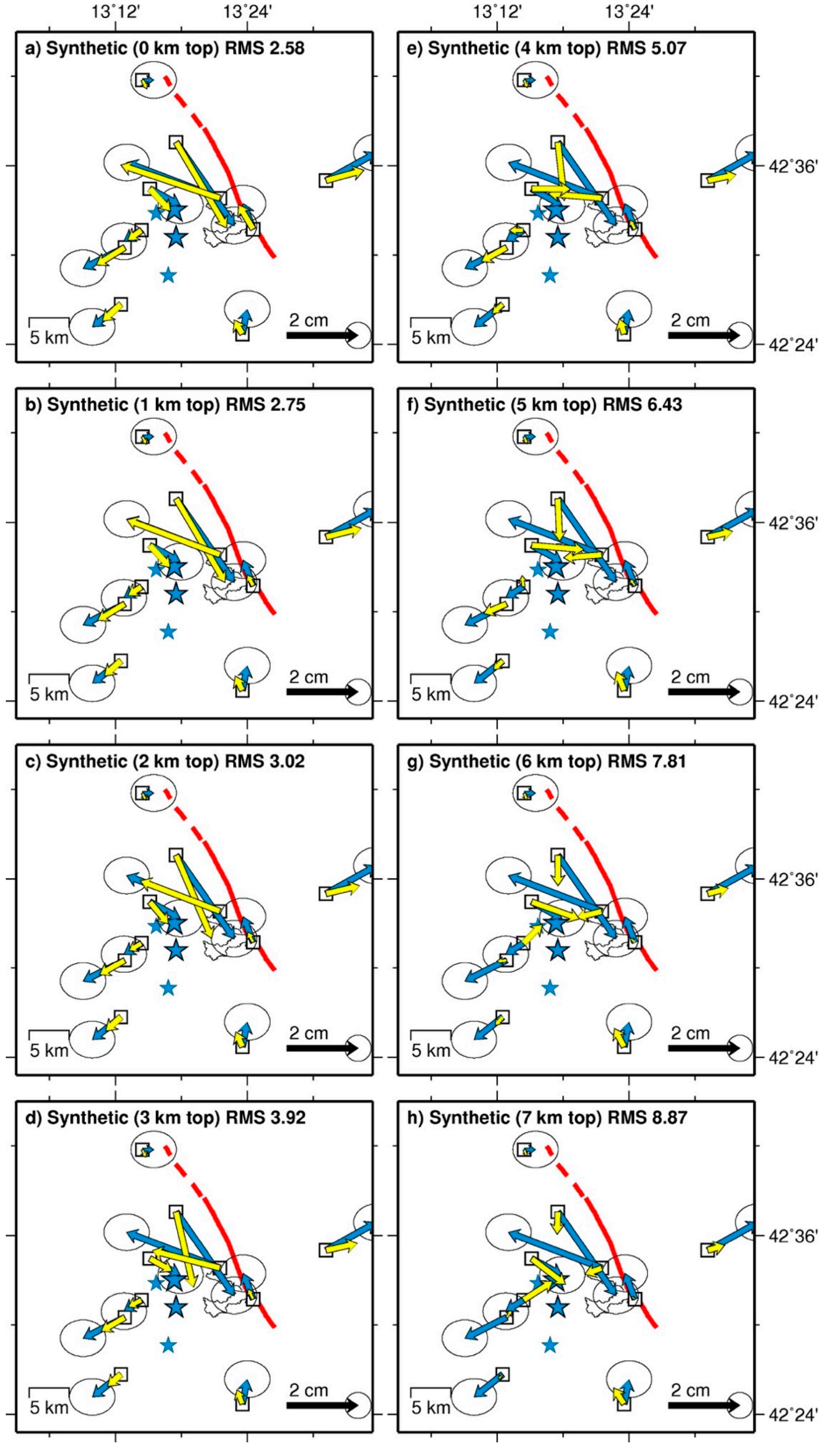

Figure 5. Fit to the horizontal components of GPS data as a function of the assumed fault top depth. Observed (blue) and modelled (yellow) cumulative GPS displacements: (**a**) horizontal, and (**b**) vertical displacements, respectively. Note that increasing the depth of the fault, significantly worsens the fit to the data. .

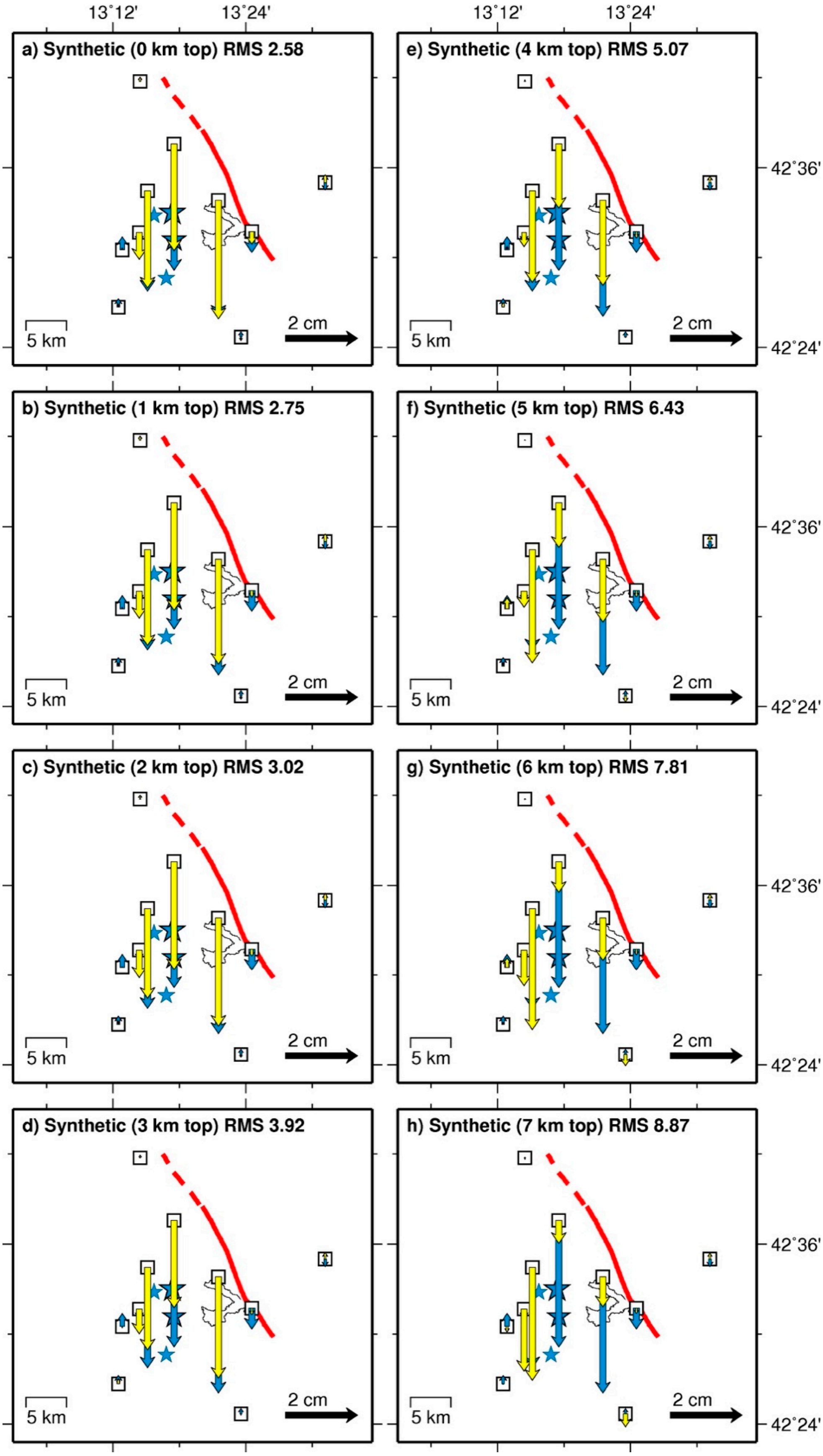

Figure 6. Fit to the vertical component of GPS data as a function of the assumed fault top depth. Observed (blue) and modelled (yellow) cumulative GPS displacements: (**a**) horizontal, and (**b**) vertical displacements, respectively. Note that increasing the depth of the fault, significantly worsens the fit to the data.

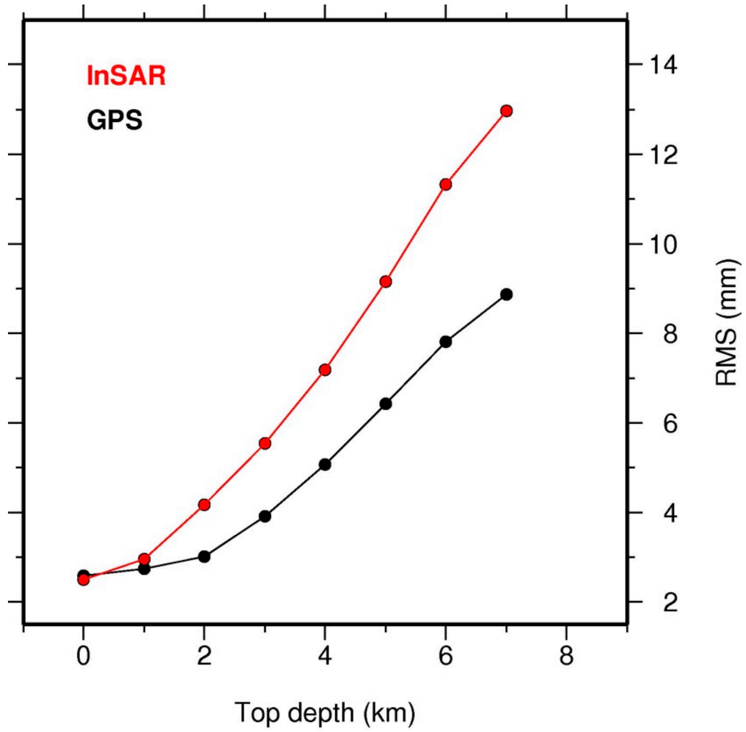

Figure 7. Trade-off curves between RMS (in mm) data reduction and assumed fault top depth. The black circles represent the RMS of the GPS datasets, while the red ones are relevant to the InSAR measurements. Note that increasing the depth of the fault, significantly worsens the fit to the data.